Elucidating the Influence of Linker Histone Isoforms on Chromatosome Dynamics and Energetics

Dustin C. Woods[1] and Jeff Wereszczynski[2,*]

[1]Department of Chemistry and the Center for Molecular Study of Condensed Soft Matter, Illinois Institute of Technology, Chicago, IL 60616
[2]Department of Physics and the Center for Molecular Study of Condensed Soft Matter, Illinois Institute of Technology, Chicago, IL 60616
[*]To whom correspondence should be addressed: jwereszc@iit.edu

June 4, 2019

Abstract

Linker histones are epigentic regulators that bind to nucleosomes and alter chromatin structures and dynamics. Biophysical studies have revealed two binding modes in the linker histone/nucleosome complex, the chromatosome, where the linker histone is either centered on or askew from the dyad axis. Each has been posited to have distinct effects on chromatin, however the molecular and thermodynamic mechanisms that drive them and their dependence on linker histone compositions remain poorly understood. We present molecular dynamics simulations of chromatosomes with two linker histone isoforms, globular H1 (GH1) and H5 (GH5), to determine how their differences influence chromatosome structures, energetics, and dynamics. Results show that both linker histones adopt a single compact conformation in solution. Upon binding, DNA flexibility is reduced and there is increased chromatosome compaction. While both isoforms favor on-dyad binding, the enthalpic benefit is significantly higher for GH5. This suggests that GH5 is more capable of overcoming the large entropic reduction required for on-dyad binding than GH1, which helps rationalize experiments that have consistently demonstrated GH5 in on-dyad states but that show GH1 in both locations. These simulations highlights the thermodynamic basis for different linker histone binding motifs, and details their physical and chemical effects on chromatosomes.

Introduction

In eukaryotes, chromosomes serve as the primary storage of genomic information within an organism and consists predominantly of organized, long condensed fibers of DNA and structural proteins.[1] These fibers are made of compacted repeating arrays of DNA-protein complexes collectively known as chromatin.[2,3] Despite being tightly condensed, chromatin still allows for enzyme induced replication, repair, and transcription.[4–6] The basic building block of chromatin fibers is the nucleosome core particle (NCP) which consists of 147 base pairs of DNA wrapped around an octameric core of histone proteins.[7] The NCP core consists of duplicates of four histones: H2A, H2B, H3, and H4.[1,8] These histones bind to one another to form H2A-H2B and H3-H4 dimers, while the H3-H4 dimers combine into a tetramer. This tetramer then combines with the H2A-H2B dimers to form the octameric core.[9,10]

The chromatosome is an extension of the NCP containing the same structural foundations with an additional ∼20 base pairs of DNA accompanied by a linker histone (LH) protein (Figure 1).[11] Colloquially known as histone H1, this nuclear protein plays a crucial role in the condensation of nucleosome chains into higher order structures,[12–15] as well as other cellular functions[14] such as gene expression,[16,17] heterochromatin genetic

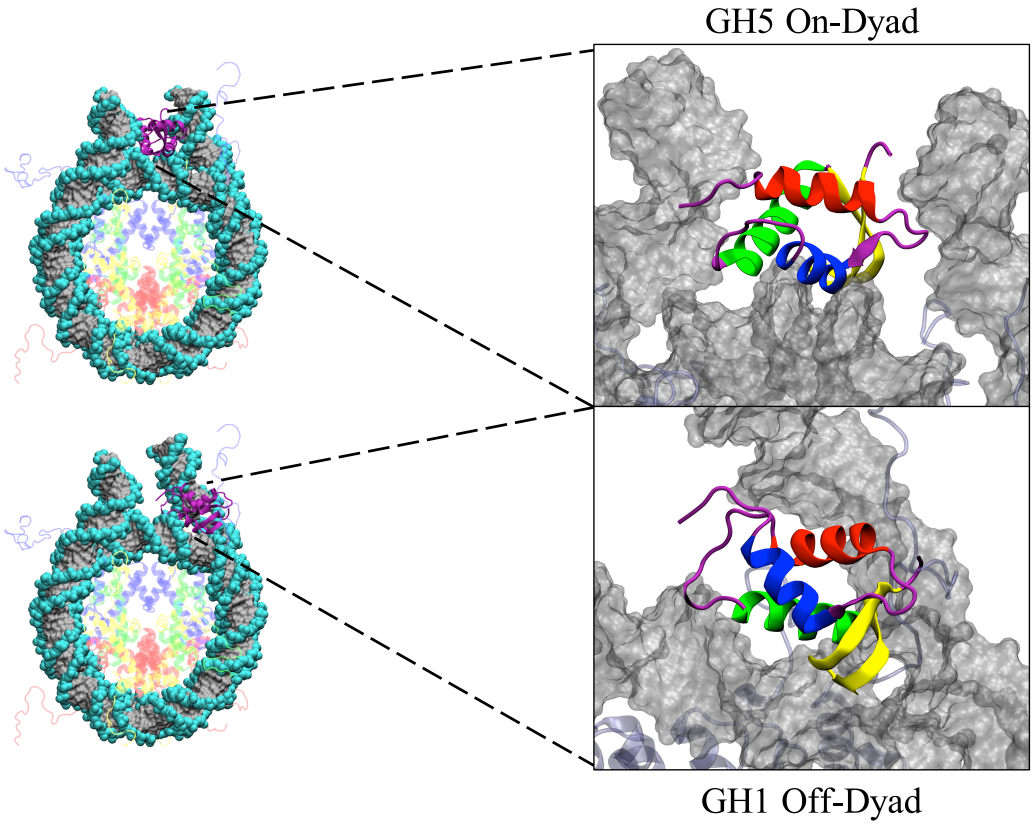

GH1 ^{43}SASHPPTQQ-MIDAAIKNLKERGGSSLLAIKKYITATYKVDAQKLAPFIKKYLKSLVVNGKLIQTKGKGASGSFKLSA^{119}
GH5 ^{22}SASHP-TYSEMIAAAIRAEKSRGGSSRQSIQKYIKSHYKVG-HNADLQIKLSIRRLIAAGVLKQTKGVGASGSFRLAK^{97}

Figure 1: On-dyad (top) and off-dyad (bottom) chromatosome structures. Global structures are shown on the left with zoomed-in figures of the linker histones GH5 (top) and GH1 (bottom) are on the right. On the left, histones are color-coded as follows: Histone H2A (yellow), Histone H2B (red), Histone H3 (blue), Histone H4 (green), Histone GH5/H1 (cyan), and DNA (gray). On the right the linker histones are colored by secondary structure: α-helix 1 (α1; red), α-helix 2 (α2; blue), α-helix 3 (α3; green), the β-sheet (yellow), and disordered regions (purple). Sequences for GH1 and GH5 are shown on the bottom, with identical residues in green.

activity,[18] and cell differentiation,[19,20] among many others.[21–23] Additionally, linker histones predominantly interact electrostatically with the backbone phosphates of DNA using positively charged residues,[24–26] which stabilizes nucleosome arrays hindering linker DNA accessibility.[15,27–30] However, this effect has shown to be completely abrogated upon the addition of nucleosome-free regions within H1-saturated arrays.[31] They are found roughly every 200 ± 40 base pairs,[32] but may be spaced more intermittently to regulate DNA accessibility for transcription factors. A distinct member of the H1-family is the H5 isoform, found in avian erythrocytes.[32]

Linker histones primarily bind to the nucleosome in two states. In the "on-dyad" location[33–35] the linker histone is centered on the dyad axis (Figure 1 (top)), whereas in the "off-dyad" configuration the histone

binds in a DNA groove off the dyad axis[36–38] (Figure 1 (bottom)). Variations in the linker histone binding mode may result in differences in the mechanical stability and overall packaging within the greater chromatin architecture, which would naturally affect the accessibility of DNA in nuclear processes.[39–41]

Several factors contribute to the thermodynamic preference for on- vs off-dyad binding in linker histones. Recent work by Zhou *et al.* examined the binding modes of wild type globular histone H1 (GH1), H5 (GH5), and a GH5 pentamutant.[36] Paramagnetic relaxation enhancement (PRE) experiments showed that GH5 binds on-dyad and that GH1 binds off-dyad, but also that a small number of mutations are able to shift the equilibrium of the GH5 binding state from on- to off-dyad.[36] This suggests that the thermodynamic balance between these states is finely tuned by specific linker histone/nucleosome contacts. These studies are supported by cryo-EM experiments of condensed nucleosome arrays which suggested an off-dyad H1 binding mode.[37] In contrast, in cryo-EM experiments of single nucleosomes, H1 has been observed in the on-dyad binding state,[34] while there is evidence to suggest that off-dyad binding in the cryo-EM map of the 30-nm fiber may be a result of cross-linker effects.[42] Taken together, these experiments paint the picture that linker histones likely bind in an ensemble of on- and off-dyad states, and that the balance of these two conformations is dictated by several factors including the linker histone primary sequence, the chromatosome's stereochemical environment, and greater chromatin architecture.[43]

The contrasting influence of linker histone isoforms on the chromatosome structure and energetics, and the extent to which they affect greater chromatin dynamics, remains unclear.[44–46] Using Brownian dynamic docking simulations, Öztürk *et al.* found that GH5 displays a range of conformational flexibility and affects the overall chromatosome dynamics, including the linker DNA.[47] With similar techniques they later showed that even slightly varied linker histone sequences, including point mutations and posttranslational modifications, can significantly affect the chromatosome structure.[43,48] Moreover, with accelerated molecular dynamics simulations they found that the GH5 β-sheet loop (β-loop), which has both an open and closed state in the crystal structure,,[49] favors the closed-state in solution, although the open-state may still be populated. This is in line with the closed-state being the only conformation observed in chromatosome crystal structures.[33,34,42] However, there is evidence suggesting that linker histones may exist in alternative conformations[50,51] and binding orientations.[50,52–54]

Despite these many excellent experimental and computational studies, several questions remain concerning linker histones and their nucleosome binding. For example, to what extent does linker histone plasticity affect its function? What are the effects of on- and off-dyad binding on chromatosome dynamics? How do specific thermodynamic forces influence the on- vs off-dyad binding equilibrium? How are these properties

influenced by different linker histone isoforms? To address these questions, we have performed a series of conventional and free energy molecular dynamics (MD) simulations of chromatosomes containing GH1 and GH5 bound in both on- and off-dyad states. Results suggest that both GH1 and GH5 readily adopt a single compact configuration. Furthermore, in the off-dyad state linker histones display increased localized sampling while modestly altering the linker DNA dynamics, while linker histones have highly stable binding in the on-dyad state while significantly restricting DNA motions. Energetic analyses shows that the equilibrium between on- and off-dyad binding is the result of a balance between Van der Waals and electrostatic interactions that is dictated by the linker histone isoform type. Together, these results suggest that, regardless of the isoform, on-dyad binding is enthalpically stabilized whereas off-dyad binding is relatively more entropically stabilized. Furthermore, when in on- and off-dyad conformations different linker histone isoforms have similar effects on chromatosome structures and dynamics, and that the role of linker histone modifications is likely to shift the relative populations between these binding states. The *in vitro* ensemble of binding modes, and therefore the greater structure of linker histone containing chromatin fibers, is therefore dictated by competing thermodynamic forces which are likely influenced by a myriad of structural and environmental factors in the nucleus.

Methods

System construction

Core histones were modelled based on the 1KX5 crystal structure (resolution 1.94 Å[55]). Widom 601 DNA[56,57] was taken from the 4QLC crystal structure, which has a lower resolution (3.50 Å) but both DNA and GH5 in an on-dyad conformation.[33] Missing residues and nucleotides were added using Modeller via the Chimera graphical user interface.[58,59] Linker histone coordinates from the 4QLC structure were used for GH5 on-dyad simulations, whereas for GH1 on-dyad simulations the GH5 primary sequence was mutated to the GH1 sequence (Figure 1). The completed on-dyad GH1 had an RMSD of 0.33 Å relative to the recently published crystallographic GH1 structure (PDB 5NL0, resolution: 5.4 Å).[34] For simulations of the NCP, the linker histone was deleted.

Off-dyad binding models were based on a combination of manual placement, rigid docking, and flexible docking. First, the exit DNA was manually adjusted to allow space for the linker histone to be placed in an off-dyad binding mode. Rigid docking of GH1 was then performed with the 12 Å cryo-EM map as a guide using the Colores module of Situs,[37,60,61] which was followed by flexible docking using internal coordinates

normal mode analysis (iMOD).[62] To validate the linker histone placement, theoretical paramagnetic relaxation enhancement (PRE) intensity ratios were calculated and compared to experimental data (see Analyses Methods below). A model of off-dyad GH5 binding was constructed by superimposing and replacing GH1 coordinates with GH5 coordinates.

Molecular Dynamics Simulations

All systems were prepared with *tleap* from the AmberTools16[63] software package. Each system was solvated in a TIP3P water box extending at least 10 Å from the solute.[64,65] The solvent contained 150 mM NaCl, sodium cations to neutralize negative charges, and magnesium ions that replaced the manganese ions in the 1KX5 crystal structure. The AMBER14SB and BSC1 force fields were used for protein and DNA interactions.[66,67] All simulations were performed using NAMD version 2.12.[68] A cutoff distance of 10.0 Å with a switching function beginning at 8.0 Å was used for nonbonded interactions, and long range electrostatics were treated with particle mesh Ewald calculations.[69] For constant pressure calculations a modified NAMD version of the Nosé-Hoover barostat was used with a target pressure of 1.01325 bar while the Langevin thermostat was with a target temperature of 300K.[70]

System were minimized twice for 5000 steps, first with a 10 kcal·mol^{-1}·Å^{-2} harmonic restraint applied to the solute and then followed by no restraints. Using the Langevin thermostat, systems were then heated in the NVT ensemble from a temperature of 10K to 300K in 1K increments every 4 ps with a 10 kcal/mol kcal·mol^{-1}·Å^{-2} solute restraint. This restraint was then reduced by 0.001 kcal/mol every 60 femtoseconds in the NPT ensemble. Equilibration runs with no restraints and a temperature of 300K were then performed. Simulations were conducted on seven systems: four chromatosomes (each containing linker histones GH1 or GH5 in either the on- and or off-dyad binding mode), one nucleosome core particle, and two isolated linker histones (GH1 and GH5). Each simulation was run in triplicate at 250 ns in length using HPC resources via the Extreme Science and Engineering Discovery Environment (XSEDE).[71]

Free-Energy Simulations Free-energy profiles of linker histones in solution were computed using extended adaptive biasing force (ABF) simulations.[72–74] Atomistic structures of GH5 in both the open- and closed- β-sheet loop (β-loop) states were acquired from the 1HST crystal structure .[49] GH1 was built using the methodology described above. MD simulation parameters were the same as described above. The distance and angle (ϕ_2) were used as collective variables, as detailed in Figure S1 of Section S4 of the Supporting Information.

ABF simulations were initiated from the open- and closed-state conformations for both GH1 and GH5.

Each system was equilibrated for 50 ns before applying the biasing force. Angular forces were accumulated in bins of a 2° width between the bounds of 0° to 180°. Distances were accumulated in bins of 0.5 Å width between 5 Å and 30 Å. The biased atoms were kept within the bounds of the reaction coordinate by implementing a 0.1 and 0.5 kcal/mol/Å^2 harmonic force at either end with an extended fluctuation of 2.5° and 5.0 Å for angles and distances, respectively. The ABF was applied for 1 μs for each starting conformation, totaling 2 μs of ABF simulations for both GH1 and GH5.

Analyses Methods

Unless otherwise stated, all analyses were performed using *cpptraj* with the first 50 ns of the trajectory excluded for equilibration.[63] Figures were created using Visual Molecular Dynamics.[75] Protein-DNA contacts were defined between the heavy atoms of residues within 4.0 Å of one another.

Estimated Binding Affinity. Binding affinities were estimated with an MM/GBSA analysis (molecular mechanics - generalized Born surface area) using the *MMPBSA.py* script from the AMBER16 software suite.[76] The three trajectory approach was implemented by using the trajectories from chromatosome simulations as the complex, the NCP simulations as the receptor, and simulations of linker histones in solution as the ligands. Explicit trajectories were stripped of all solvent molecules while using trajectory frames every 4 ps. The implicit solvent model, *GBneck2* with the *mbondi3* radii parameters were used as they have been shown to have good agreemenet with more expensive Poisson–Boltzmann calculations for protein/nucleic-acid complexes.[77] The salt concentration was set to 150 mM.

Clustering. Binding modes of GH1 and GH5 were compared by calculating RMSD values of the helical α-carbons in the linker histone with respect to the helical α-carbons in the core histones. The RMSD analysis was limited to the helical α-carbons to reduce noise from the loops and intrinsically disordered tails. Based on the RMSD results, a cutoff of 2.0 Å was chosen for the subsequent clustering analysis (Figure S2). Clustering was performed using the hierarchical agglomerative approach implemented in the *cluster* module of *cpptraj* from the the AmberTools16 software package.[78]

Linker DNA Dynamics. The the in- and out-of nucleosomal motions of the linker DNA were quantified to describe the linker DNA motions. To define the plane, the nucleosomal DNA was divided into four quadrants and the center of mass of the C1' atoms within the two quadrants located distal from the linker DNA were used for two points, while the third point was defined as the C1' center of mass of bases 83 and 250 which are located approximately on the dyad axis. The linker DNA vectors were defined as the C1' center of mass of the base pairs at the origin of the linker DNA (bases 20-315 and 148-187) and terminal base

pairs (bases 1-334 and 167-168), respectively. The α-angles were defined as in-plane and the β-angles were defined as out-of-plane motions of this vector. Positive α-angles were defined as inward motions towards the dyad axis while positive β-angles were defined as outward motions away from the nucleosomal-plane. For reference, the angles shown in Figure 6 are positive.

The normalized mutual information (NMI) between angles was calculated to determine the correlations between each pair of angles.[79] The NMI has the advantageous property that all values are in the range of 0 to 1 and are therefore easier to interpret than standard mutual information (MI). For detail discussion of the NMI see Supporting Information. The change in sampling of bound linker histones from the NCP were computed by the Kullback–Leibler divergence utilizing the NCP sampling distributions as the reference set:[80]

$$D_{KL}(P\,||Q) = -\sum_{x\in X} P(x) log\left(\frac{Q(x)}{P(x)}\right) \tag{1}$$

where $Q(x)$ is the normalized reference distribution (nucleosomal linker DNA angles) and $P(x)$ is the normalized data set (chromatosomal linker DNA angles).

Paramagnetic relaxation enhancement (PRE) intensity ratios. Theoretical paramagnetic relaxation enhancement (PRE) cross-peak intensity ratios were estimated based on distances between experimentally labelled histone core (H2A T119 and H3 K37) and linker histone methyl-terminated residues.[36,38] Since our simulations did not include the MTSL probe, wild type residues were used for distance calculations, similar to Piana *et al.*[81] For the K37 probe, distances were measured from the lysine terminal nitrogen to the terminal methyl carbon atom of each respective residue, while the T119 distance was measured from the threonine terminal methyl carbon. Note, that each of these neutral residues have two distinct methyl groups and were referred to as *methyl-a* and *methyl-b*. Using these distances, the predicted intensity ratios where calculated using known equations and the average of the *methyl-a* and *methyl-b* values were used to compared to experimental values.[36,38,55] Briefly, the relationship between the interatomic distances and the paramagetic relaxation cross peak intensity ratios was calculated as:[82,83]

$$\frac{I_{ox}}{I_{red}} = \frac{e^{\beta(r+d)^{-6}}}{1+\alpha(r+d)^{-6}} \tag{2}$$

where $\alpha = 4.5\times10^8$, $\beta = 3.4\times10^7$, and d = 9.0 Å, a correction factor based on the experimental calibration curve (see Section S2 of the Supporting Information for more details).[33,36,38]

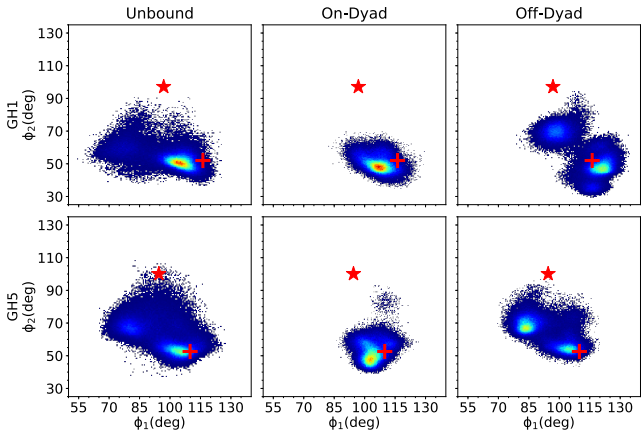

Figure 2: Flexibility of the β-loop using ϕ-angles inspired by a previous study.[47] Shown are 2D-histograms of ϕ_2 versus ϕ_1 angles (deg) in the unbound (left), on-dyad (middle), and off-dyad (right) states. Density ranges from blue (lower) to red (higher). The red cross corresponds to the initial values of the closed-state linker histone, while the red star corresponds to the open-state values.

Results

Unbound Linker Histones Favor the Closed-State

To quantify the dynamics of linker histones in solution, we measured two angles over our unbound GH1 and GH5 simulations, ϕ_1 and ϕ_2, which were inspired by previous work on GH5 by Ozturk *et al.* (Figure 2, left side).[47] In that work, GH5 was shown to preferentially adopt the closed conformation in solution, although the open-state was sampled in accelerated MD simulations. Similarly, our unbound GH1 and GH5 simulations predominantly sampled closed β-loop states. ϕ_1 displayed a wider distribution than ϕ_2 and often included values associated with both the open- and closed-states. For example, in GH1 simulations there was a spread of ϕ_1 from 54.6° to 125.4°, which encompasses both the crystolgraphic closed and open values of 116.2° and 96.9°, respectively. However, ϕ_2 angles were more indicative of β-loop dynamics with average values of 52.6° ± 5.2° and 60.2° ± 8.9° for GH1 and GH5, both of which correspond to closed states. Therefore, ϕ_2 appears to be a stronger metric of β-loop structures, whereas ϕ_1 is subject to increased mobility throughout the β-sheet.

To quantify the dynamics of the β-loop, adaptive biasing force (ABF) simulations were performed to determine the relative stability of the open-state in solution. Initial attempts at using ϕ_1 and ϕ_2 as dual collective variables resulted in PMF convergence issues due to the previously mentioned poor discriminatory ability of ϕ_1. Therefore, we used ϕ_2 and the distance between the β-loop and helix α3. However, these collective variables proved to be highly correlated to one another (Figure S3). Consequently, here we report

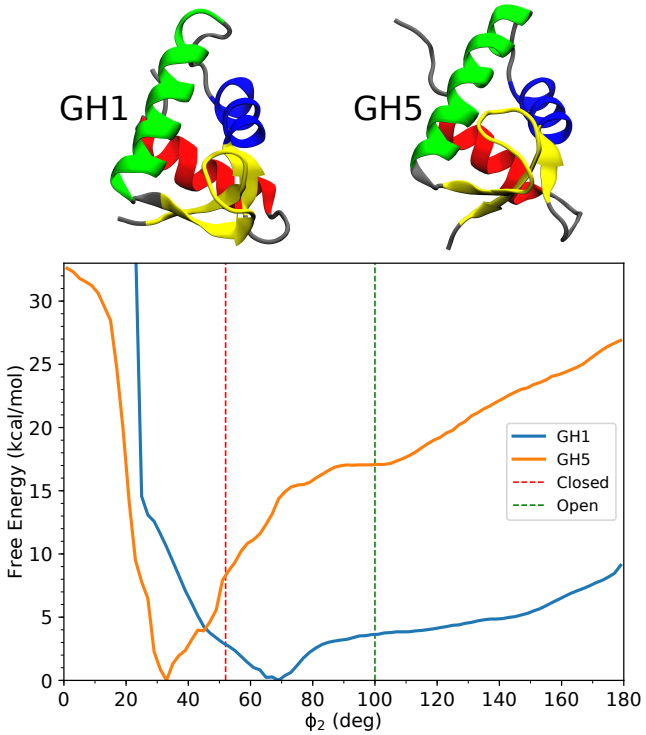

Figure 3: Potential of mean force from ABF simulations showing the relative free-energy landscapes between GH1 and GH5 along the ϕ_2 coordinate space. The red dotted-line corresponds to the closed-state angle, $\phi_2 = \sim 52.0°$, while the green dotted-line corresponds to the open-state angle, $\phi_2 = \sim 100.0°$, of the crystalographic closed-state from 1HST.

the projection of the two-dimensional potential of mean force (PMF) along the one-dimensional ϕ_2 coordinate space (Figure 3).

The PMF shows that both GH1 and GH5 contain a single free-energy well GH5 favors a more compact state than GH1. The GH5 ϕ_2 minimum is located at 33.0° and more compact than the crystallographic closed-state at 52.0°. The GH1 ϕ_2 minimum is more extended at 69.0°, yet below the crystallographic open-state at 102.0°. Additionally, GH1 presents a broad free-energy surface, where the probability of sampling wider ϕ_2 angles is greater than GH5. The free-energy along the PMF of GH1 and GH5 at the ϕ_2 angle from the crystallographic open-state was 3.70 kcal/mol and 17.1 kcal/mol, respectively, indicating that it is sparsely populated in solution for both linker histones.

The free-energy minima of GH1 and GH5 were characterized by clustering structures from the ABF simulations along the ϕ_2 coordinate space. Visually, both GH1 and GH5 structures correspond to the closed-state of the β-loop, despite a respective -19.0° and +17.0° deviation from the crystallographic reference. Additionally, we clarify that while the angular extent of the closed-state may vary by ± 19.0°, the open-state

should have a more ambiguous definition of >83.0°.

Bound Linker Histone Dynamics

Off-Dyad Linker Histones Sampled Multiple States in the DNA Binding Pocket

There is no reported high-resolution crystal structure for linker histones bound in an off-dyad state. Therefore, a model for off-dyad GH1 was constructed based on both the low-resolution cryo-EM map of a poly-nucleosomal array by Song *et al.* and NMR paramagnetic relaxation enhancements (PRE) experiments by Zhou *et al.* (see methods).[36,38] The GH5 off-dyad model was constructed by mutating the GH1 model to the appropriate primary sequence. To verify this model was in concordance with the available experimental data, we compared our initial structures to data from Zhou's PRE experiments. To make a direct comparison to the experimental data, we estimated the observed PRE intensity ratios (I_{ox}/I_{red}) using distances between the histone core labeled probed residues H2A T119 and H3 K37 and GH1 methyl-terminated residues (Figure 4). In general, we observed suitable agreement for both sites, with mean signed errors of 0.02 and 0.04 for the T119 and K37 probe sites, respectively. Based on these results, we found the off-dyad structures of GH1 and GH5 sufficient to begin simulations.

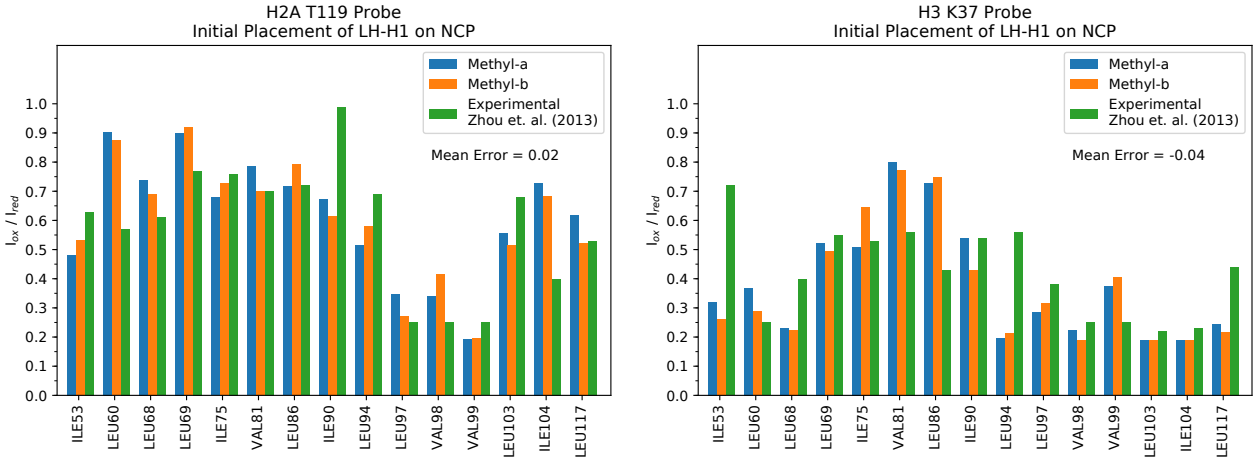

Figure 4: Theoretical paramagnetic relaxation enhancement intensity ratios (I_{ox}/I_{red}) for the initial placement of the linker histone GH1 onto the extended nucleosome core particle for probe residues H2A T119 and H3 K37. Each residue contains two terminal methyl groups labeled methyl-a (blue) and methyl-b (orange), while experimental results (green) show only a solitary signal. The mean error is given in the top right-hand corner of each graph.

For both GH1 and GH5, there was considerably more sampling of the linker histone position in the off-dyad initial placement relative to on-dyad. This is exhibited by increased root-mean-square deviation (RMSD) values in off-dyad simulations (Figure S2). This contrast in RMSD values between binding modes

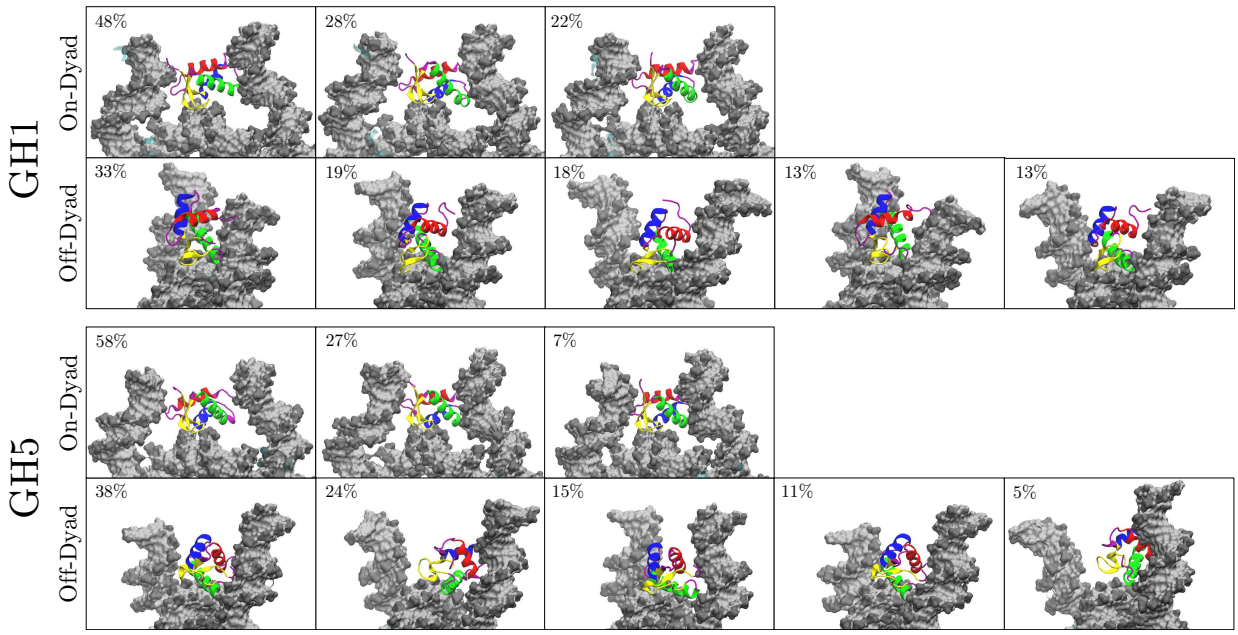

Figure 5: Representative snapshots of clusters for linker histones GH1 and GH5 in both the on- and off-dyad binding modes. Shown are clusters totalling at least the top 90% of frames analyzed. The respective percentage of each cluster is provided in the top left-hand corner of each snapshot.

is reflected in a clustering analysis which demonstrates that off-dyad systems have more clusters that are less populated than on-dyad systems (Figure 5). More specifically, when clusters were separated by 2 Å from one another, six clusters were found for GH5 in an on-dyad binding mode whereas 11 were found for off-dyad GH5. Similarly, six and eight cluster were found for GH1 on-dyad and off-dyad. However, some of these clusters had a low population, and when the clusters representing only the top 90% of frames were analyzed this resulted in three clusters for each on-dyad and five clusters for each off-dyad linker histone (Figure 5). These suggest that off-dyad linker histones are more fluid in the DNA pocket. In contrast, the increased number of linker histone-DNA contacts in the on-dyad pocket (discussed below) leads to a more confined and rigid complex, hence decreased sampling.

This increased sampling in off-dyad systems contributes to increased uncertainty in the GH1 observed time-averaged PRE ratios (Figure S4). These values had a higher discrepancy to experiments with mean errors of 0.11 and 0.16, although for most residues the experimental values were within the 80% confidence interval of the simulation derived ratios (Figure S4). Some of these differences are likely due to localized fluctuations of the linker histones that occur throughout the simulations and the fact that distance changes on the order of 2-3 Å in methyl/probe distances can result in difference on the order of 0.10-0.15 in the PRE intensity ratio.

In all bound linker histones simulations the β-loop remained in the closed conformation. This is exemplified by the ϕ_2 angle distributions, which were 49.7° ± 4.2° and 55.0° ± 11.5° for GH1 in on- and off-dyad states, and 52.4° ± 5.6° and 63.7° ± 7.9° for GH5 on- and off-dyad systems (Figure 2). As previously noted, ϕ_1 is a relatively poor metric to distinguish between the open- and closed β-loop states.

On-Dyad Binding Restricts DNA Motions

Linker histones interact with both the nucleosomal and linker DNA, which has a direct effect on their motions within the DNA binding pocket. Above, we have emphasized the importance of this interaction by showing how the linker histone binding pose affects experimental results. To further probe these dynamics, we measured the in and out of nucleosomal-plane motions of both linker DNA arms, which are termed here as the α and β angles for the entry and exit DNA, as inspired by Bednar *et al.*[34] (see Figure 6 for definitions). The α angles correspond largely to DNA breathing motions, and over all simulations ranged from 0.0° to 54.0° with an average value of 25.0°. The lack of negative α angles indicates that on the timescales sampled here, no significant opening of the DNA was observed. Out-of-plane linker DNA fluctuations, described by β angles, ranged from -27.4° to 32.1° in all simulations, similar in scope to the α angles.

Linker histone binding has a significant effect on both the equilibrium distributions of these motions as well as their correlations to one another. In addition to the 2D-histograms of the α and β angles (Figs. 6 and S5-S6), their correlations were analyzed by computing the normalized mutual information (NMI) for each angle pair (Table 1), and the changes induced by linker histone binding were quantified with the Kullback-Leibler (KL) divergence for each probability distribution relative to the NCP (Tables 2 & 2). Of particular note are the α-entry/α-exit angle distributions which highlight the breathing motions of both DNA ends (Figure 6, middle). In this space, the nucleosome samples a wide range of angles in both the entry and exit DNA with little correlation between the two as shown by the NMI value of 0.04. In off-dyad binding there is a similar range of motions for GH1, which has a KL divergence of only 1.62 to the NCP state, while GH5 has a similar range of sampled states with a shifted mean, resulting in a higher KL value of 3.95. For both cases the correlations between the α angles are relatively low, with a modest increase in the NMI values for GH1 and a slight decrease for GH5. In contrast, on-dyad binding shows a significant reduction in the α-entry/α-exit conformational space, as the range of motion of both the entry and exit DNAs are substantially restricted regardless of the linker histone isoform. The KL divergences for these states are high, 4.35 and 5.82 for GH1 and GH5, and the correlations for each state are approximately three times higher than for the NCP.

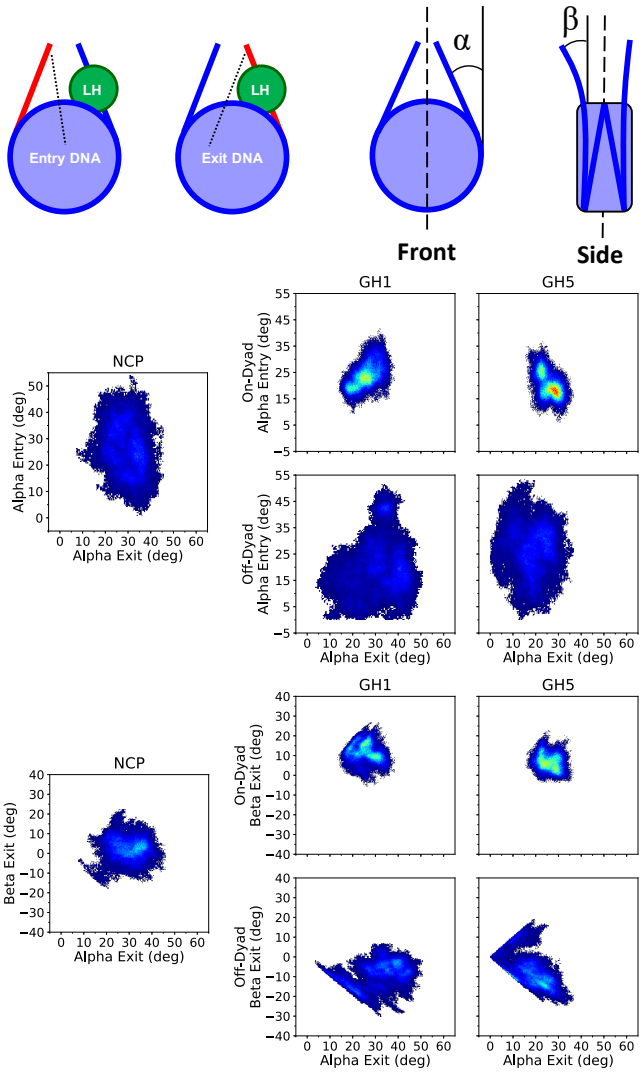

Figure 6: Density plots of linker DNA α and β angles. Entry and Exit DNA (from left to right) are defined in the top left graphic. The linker histone (LH) is shown in green, the linker DNA arm in red, while the rest of the nucleosome is blue. To the right are the α and β definitions (from left to right), which were inspired by Bednar *et al.*[34] The dyad axis is shown as a black dotted line. Each plot shows a 2D histogram of the entry linker DNA angles versus the exit linker DNA angles for both α (middle set of plots) and β (bottom set of plots) angles, with density ranges from dark blue (lowest) to red (highest). Each plot contains the linker DNA from the nucleosome core particle along with GH1 and GH5 in the on- and off-dyad binding modes.

Another distribution of interest is the α-exit/β-exit phase space, which describes the in- and out-of-plane motions of the exit DNA (Figure 6, bottom). In the canonical nucleosome the average α-exit and β-exit angles are 30.5° and -2.7° respectively, indicating that this DNA arm fluctuates about states that are slightly pointing inward when viewed from the side. These motions are largely uncorrelated, with an NMI value of 0.03. Binding in the off-dyad location has a dramatic effect, forcing the DNA outward and

Table 1: Normalized mutual information values for DNA motions. Values in parenthesis are the increase in the mutual information for that measurement over the canonical nucleosome.

Linker Histone	Position	α-Entry/α-Exit	α-Entry/β-Entry	α-Exit/β-Exit	β-Entry/β-Exit
None		0.04	0.05	0.03	0.02
GH1	On-Dyad	0.12 (2.99)	0.29 (5.46)	0.08 (2.81)	0.04 (2.21)
	Off-Dyad	0.08 (1.96)	0.17 (3.25)	0.12 (4.19)	0.08 (3.80)
GH5	On-Dyad	0.13 (3.24)	0.16 (2.99)	0.04 (1.41)	0.06 (2.98)
	Off-Dyad	0.03 (0.82)	0.09 (1.72)	0.18 (6.41)	0.07 (3.50)

shifting the β-exit angles to fluctuate around 9.5° and 7.1° for the GH1 and GH5 systems. This alters the sampling distributions, with KL values of these angles of 6.33 and 9.48 for GH1 and GH5, and increasing the correlations between the motions by four to six fold. In contrast, on-dyad binding decreases the average β-exit value to -12.1° and -6.1° for GH1 and GH5 as this binding mode pulls the DNA inward from the side view. This results in more modest changes to the α-exit/β-exit phase space and lower correlation increases over the NCP.

Table 2: Kullback-Leibler divergence values for two dimensional probability distributions of DNA. Cells are colored on a scale from blue (lower) to white to red (higher).

Linker Histone	Position	α-Entry/α-Exit	α-Entry/β-Entry	α-Exit/β-Exit	β-Entry/β-Exit
GH1	On-Dyad	4.35	5.55	4.56	5.52
	Off-Dyad	1.62	1.75	6.33	6.11
GH5	On-Dyad	5.82	5.12	3.01	1.91
	Off-Dyad	3.95	1.58	9.48	3.36

In contrast to the exit DNA, the entry DNA is largely unaffected by off-dyad binding with KL values below 1.8 relative to the NCP. On-dyad binding creates a larger perturbation, with KL values above 5.1 as ranges of motion of both angles are restricted relative to the NCP. The average β-exit angles have a slight increase from -5.1° in the NCP to 1.8° and 0.6° in GH1 and GH5, which are both significantly greater than the values in the exit DNA. Together, this creates an asymmetry in the profile view of DNA structures, as illustrated in Figure S5.

Table 3: Free-energy difference (kcal/mol) between on and off-dyad binding states as estimated by MM/GBSA analysis. A negative value indicates more favorable binding in the on-dyad state.

Linker Histone	Binding Mode	ΔE_{total}	$\Delta E_{internal}$	ΔE_{elec}	ΔE_{VdW}	$\Delta\Delta E_{total}$	$\Delta\Delta E_{internal}$	$\Delta\Delta E_{elec}$	$\Delta\Delta E_{VdW}$
GH1	On-Dyad	-174.6 ± 37.0	-18.1 ± 32.5	-59.5 ± 27.2	-97.0 ± 23.9	-89.9 ± 39.0	-29.1 ± 33.3	-92.9 ± 29.4	32.1 ± 25.6
	Off-Dyad	-84.5 ± 39.9	11.0 ± 33.1	33.4 ± 28.3	-128.9 ± 23.6				
GH5	On-Dyad	-221.6 ± 37.8	-13.4 ± 32.2	-61.9 ± 24.7	-146.4 ± 24.4	-163.3 ± 36.3	-3.3 ± 33.0	-69.0 ± 22.8	-91.0 ± 24.5
	Off-Dyad	-58.2 ± 36.5	-10.1 ± 33.1	7.1 ± 24.2	-55.3 ± 22.0				

Table 4: Energy difference (kcal/mol) between binding species while in the complex state and unbound state as estimated by MM/GBSA analysis. A negative value (-) indicates a favorability of the binding species in complex, as oppose to an isolated state, positive (+). Full binding energies for each state are given in Table 1

Linker Histone	Binding Mode	Binding Species	$\Delta\Delta E_{tot}$	$\Delta\Delta E_{int}$	$\Delta\Delta E_{ele}$	$\Delta\Delta E_{VdW}$
GH1	On-Dyad	NCP	-74.8 ± 25.0	-15.9 ± 23.0	-81.1 ± 20.0	22.2 ± 17.7
		LH	17.9 ± 5.2	-2.3 ± 5.0	13.3 ± 2.8	6.8 ± 3.0
	Off-Dyad	NCP	-40.3 ± 29.2	8.4 ± 23.6	-29.1 ± 20.7	-19.6 ± 16.4
		LH	28.2 ± 5.6	2.5 ± 4.9	1.7 ± 2.9	24.0 ± 3.5
GH5	On-Dyad	NCP	-95.8 ± 26.0	-12.0 ± 22.8	-74.6 ± 16.5	-9.2 ± 17.8
		LH	7.4 ± 5.0	-1.4 ± 4.9	17.0 ± 3.1	-8.1 ± 2.7
	Off-Dyad	NCP	5.7 ± 24.8	-16.8 ± 24.0	-44.9 ± 15.3	67.5 ± 15.5
		LH	10.6 ± 5.3	6.6 ± 5.0	-2.9 ± 2.8	6.8 ± 2.9

Energetic Contributions

On-Dyad Binding is Enthalpically Favored

Although both linker histones have similar physical effects on the nucleosome when bound in on- or off-dyad locations, the difference between their binding energetics determines their *in vitro* binding mode preference. To estimate binding affinities, we have used an MM/GBSA analysis to decompose the overall binding affinity into the energetic components that drive this interactions.[84] Regardless of the isoform, on-dyad binding was found to be significantly more energetically favorable than off-dyad binding (Table 3). GH5 favored the on-dyad state over off-dyad by -163.3 ± 36.3 kcal/mol, while GH1 only favored on-dyad by -89.9 ± 39.0 kcal/mol. This difference in $\Delta\Delta E_{total}$ values was largely driven by Van der Waals (VdW) interaction energies, with GH5 favoring the on-dyad state by -91.0 ± 24.5 kcal/mol and GH1 favoring off-dyad state by 32.1 ± 25.6 kcal/mol. In contrast, GH1 favors the on-dyad binding mode more than GH5 in the electrostatic interaction energies. However, a large overlap in the errors between isoforms suggests that both systems have a relatively similar electrostatic on-dyad binding preference. We emphasize that MM/GBSA approach includes a number of approximations and do not include important thermodynamic quantities such as conformational entropy or explicit solvent thermodynamics, therefore these values should be taken as qualitative estimates of binding affinities.[85,86]

Van der Waals Interactions Drive Binding Mode Selectivity

Differences between the bound and unbound binding modes suggest that a combination of electrostatic and VdW interactions from both linker histones and nucleosomes drive the system conformations (Table 4). The $\Delta\Delta E_{tot}$ of GH1 for on-dyad (17.9 ± 5.2 kcal/mol) and off-dyad (28.2 ± 5.6 kcal/mol) is ∼2.5-fold greater than GH5 on-dyad (7.4 ± 5.0 kcal/mol) and off-dyad (10.6 ± 5.3 kcal/mol). These variations are

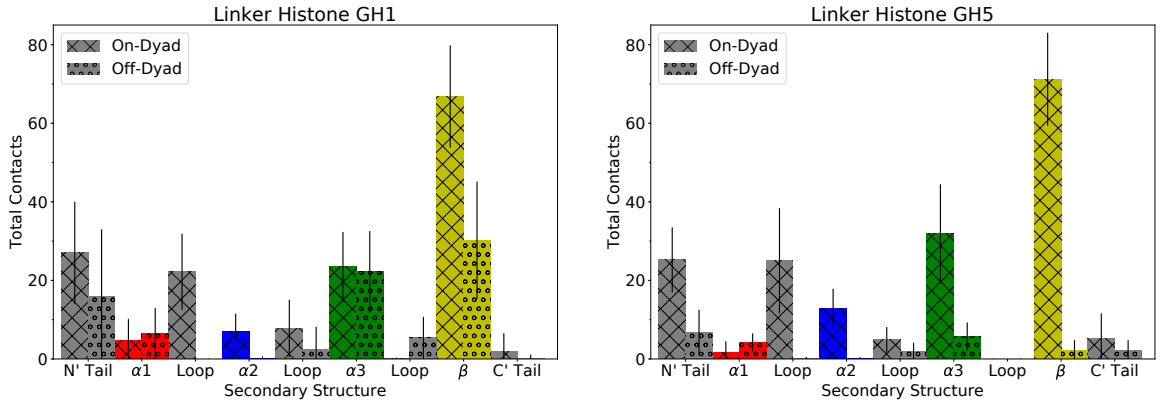

Figure 7: Total contacts of GH1 and GH5 secondary structure with DNA. The secondary structure is broken down into the following: alpha helix α1 (red), alpha helix α2 (blue), alpha helix α3 (green), β-sheet (yellow), N-terminal tail (grey), C-terminal tail (grey), and three loops (grey).

largely defined by differences in the VdW interactions where the $\Delta\Delta E_{VdW}$ of GH5 is 14.9 kcal/mol and 17.2 kcal/mol more favorable than GH1 for on- and off-dyad systems, respectively. Additionally, it is worth noting that electrostatic interactions ($\Delta\Delta E_{ele}$) for both linker histones actually favor the off-dyad complex by 11.6 kcal/mol and 19.9 kcal/mol for GH1 and GH5, respectively.

Off-dyad nucleosomes showed an increased stability when bound to GH1 over GH5 with a $\Delta\Delta E_{tot}$ of -40.3 ± 29.2 kcal/mol and 5.7 ± 24.8 kcal/mol for GH1 and GH5 systems, respectively. This contrast in $\Delta\Delta E_{tot}$ can be also be attributed to the VdW energies with $\Delta\Delta E_{VdW}$ values of -19.6 ± 16.4 kcal/mol and 67.5 ± 15.5 kcal/mol for GH1 and GH5 systems, respectively.

Contacts between linker histones and the DNA show that most on-dyad interactions come from the β-sheet (Figure 7), with 66.8 ± 12.9 and 71.2 ± 11.8 contacts for GH1 and GH5. However, the contrast between isoforms becomes more evident in the off-dyad binding mode with 30.2 ± 14.8 and 2.2 ± 2.6 β-sheet-DNA contacts for GH1 and GH5, respectively. A similar relationship is also observed in the off-dyad α3 helix and N'-tail. The GH1 α3 helix in the off-dyad binding mode has 16.4 ± 10.8 more contacts than GH5 while the N'-tail has 9.1 ± 18.0 more contacts. Combined, these additional contacts between GH1 and DNA correlate with its VdW-driven preference for off-dyad binding over GH5. Taken together, these results suggest that while on-dyad binding is energetically preferred in both isoforms, GH1 will have a higher propensity for sampling the off-dyad state than GH5, which is largely due to the difference in contacts between the β-sheet and the DNA.

Discussion

Here, we have used a combination of conventional and free energy molecular dynamics simulations to probe the effects of linker histone binding on chromatosome structures and dynamics. ABF calculations show that for both GH1 and GH5 the closed state is thermodynamically favorable, which is consistent with the GH5 aMD results of Öztürk *et al.*[47] This suggests that the open state in the 1HST crystal structure is stabilized by crystal packing forces, as exemplified by the fact that the β-loop is tucked into a hydrophobic pocket in the neighboring unit. These results are in general agreement with crystal structures of linker histones bound in the on-dyad state which have the β-loop in the closed-state.[33,34,42]

Given that there is no high resolution crystal structure of off-dyad binding, the precise binding structure and orientation of linker histones in this pocket remains inconclusive.[36,38] We therefore constructed a model of the off-dyad state based on manual placement and docking into the 30-nm cryo-EM structure by Song *et al.* which we found had generally good agreement with the PRE data from Zhou *et al.*[36,37] Based on our ABF simulations we used the closed-states of the β-loops in these structures. As highlighted by the clustering results in Figure 5, our simulations show that both linker histones are significantly more fluid in the off-dyad DNA binding pocket relative to on-dyad. This is in line with the results of Brownian dynamics docking studies from the Wade group in which they found that GH1, GH5, and assorted mutants can bind in a variety of sequence dependent orientations.[48] Furthermore, these series of simulation results would suggest transitions between on- and off-dyad states might be facilitated by multiple stable binding orientations along the DNA and encouraged by additional linker histone conformational freedom in the binding pocket.

One of the central mechanisms by which linker histones inhibit transcription and promote the compaction of chromatin fibers is by altering linker DNA dynamics. Our simulations have shown that one of the primary differences in on- and off-dyad binding is that on-dyad binding drastically restricts both the entry and exit DNA segments, whereas off-dyad binding has a distinct influence on the exit DNA dynamics with little change to the entry DNA. The latter is in line with previous Brownian and molecular dynamics simulations from the Wade group which have shown that GH5 modifies linker DNA motions in off-dyad binding modes.[47,50] Furthermore, our results indicate that these effects are largely independent of linker histone isoform type. These differences in DNA dynamics have broad implications for greater chromatin structures. For example, Mishra and Hayes have highlighted how the stoichiometric binding of H1 to nucleosome arrays can severely limit linker DNA accessibility to trans-acting factors.[31] As an additional effect of on- and off-dyad binding, Perišić *et al.* recently showed with a highly coarse-grained model that the distinct positioning of the linker histone tails in these states impacts greater chromatin structures, with off-dyad linker histones creating more

condensed chromatin fibers.[41] In light of these results, it is likely that *in vitro* on-dyad mono-chromatosomes are a result of additional linker histone DNA contacts which may not be as prevalent in condensed nucleosome arrays due to limited linker DNA conformational freedom.[34]

Given that GH1 and GH5 have similar effects on the structure and dynamics of chromatin when bound in on- and off-dyad locations, what is the role of various linker histone isoforms and modifications *in vitro*? Results from our energetic and contact analyses show that while they have similar structures, the GH1 and GH5 isoforms have drastically different energetic preferences for the on- and off-dyad states. Indeed, while both have an enthalpic preference for on-dyad binding, the preference is significantly reduced for GH1. Given that off-dyad binding is likely entropically favored due to the increased DNA and linker histone motions observed in this state, the overall free energy difference between on- and off-dyad states for GH1 appears to favor the off-dyad state more than GH5. This is in line with experimental results that consistently show GH5 in the on-dyad state, but that have provided evidence for GH1 in both the on- and off-dyad states.[34,37,42] More specifically, we observe that this change in energetic preference between the two states is driven by increased β-sheet, α3-helix, and N-terminal tail contacts in GH1 off-dyad systems. Surprisingly, these change in contacts contribute mostly to difference in Van der Waals interactions, highlighting their often overlooked influence in protein-DNA binding thermodynamics. The increased plasticity of GH1 observed in our ABF calculations may allow it to more easily deform in the context of the chromatosome, which could create more consistent and favorable contacts between GH1 and DNA. However, sustaining similar DNA contacts with GH5 may prove to be more difficult due to its more rigid tertiary structure within the highly dynamic off-dyad environment. In the context of the chromatin fiber, GH1 could prove to be "stickier" in more condensed arrays, while GH5 may provide additional stability during transcription processes when on-dyad binding is more populated.[41]

Overall, our study builds on notions of an ensemble of linker histone binding states within a highly dynamic chromatin fiber while emphasizing the contrasting influence of their isoforms on those structures and dynamics. Currently, the relative populations of these states within chromatin are still debatable. We subscribe to the hypothesis that the on- and off-dyad binding modes exist as an ensemble of states within chromatin fibers.[43] The relative populations of these states *in vivo* are likely due to a balance of not only the linker histone/nucleosome interactions examined here, but also factors outside the scope of this study such as DNA sequence and the greater chromatin architecture. Potentially, coarse-grained models may be more adept at sampling the populations of binding states in mono- and poly-chromatosomes arrays. However, care should be taken in these models as the estimated binding energies calculated here demonstrate the

importance of Van der Waals interactions within the chromatosome in addition to the more commonly considered electrostatic energies. Therefore, we emphasize that any model which attempts to recapitulate the physics underlying linker histone binding must carefully balance their electrostatic and Van der Waals components.

Acknowledgments

The authors thank Dr. Francisco Rodríguez-Ropero for his assistance in preparing the off-dyad chromatosome system and Mr. Joseph Clayton for his assistance with many aspect of the simulation analysis. This work used the Extreme Science and Engineering Discovery Environment, which is supported by the National Science Foundation [ACI-1053575].

Funding

Work in the Wereszczynski group is funded by the National Science Foundation [CAREER-1552743] and the National Institutes of Health [1R35GM119647].

References

[1] Kornberg, R. D. Chromatin structure: a repeating unit of histones and DNA. *Science* **1974**, *184*, 868–871.

[2] Olins, A. L.; Olins, D. E. Spheroid chromatin units (v bodies). *Science* **1974**, *183*, 330–332.

[3] Kaplan, N.; Moore, I. K.; Fondufe-Mittendorf, Y.; Gossett, A. J.; Tillo, D.; Field, Y.; LeProust, E. M.; Hughes, T. R.; Lieb, J. D.; Widom, J. et al. The DNA-encoded nucleosome organization of a eukaryotic genome. *Nature* **2009**, *458*, 362–366.

[4] Klemm, S. L.; Shipony, Z.; Greenleaf, W. J. Chromatin accessibility and the regulatory epigenome. *Nat. Rev. Genet.* **2019**, *20*, 207–220.

[5] Lai, W. K. M.; Pugh, B. F. Understanding nucleosome dynamics and their links to gene expression and DNA replication. *Nat. Rev. Mol. Cell Biol.* **2017**, *18*, 548–562.

[6] Koyama, M.; Kurumizaka, H. Structural diversity of the nucleosome. *J. Biochem.* **2018**, *163*, 85–95.

[7] Luger, K.; Mader, A. W.; Richmond, R. K.; Sargent, D. F.; Richmond, T. J. Crystal structure of the nucleosome core particle at 2.8 A resolution. *Nature* **1997**, *389*, 251–260.

[8] McGinty, R. K.; Tan, S. Nucleosome structure and function. *Chem. Rev.* **2015**, *115*, 2255–2273.

[9] Cutter, A. R.; Hayes, J. J. A brief review of nucleosome structure. *FEBS Lett.* **2015**, *589*, 2914–2922.

[10] Zhou, K.; Gaullier, G.; Luger, K. Nucleosome structure and dynamics are coming of age. *Nat. Struct. Mol. Biol.* **2019**, *26*, 3–13.

[11] Noll, M.; Kornberg, R. D. Action of micrococcal nuclease on chromatin and the location of histone H1. *J. Mol. Biol.* **1977**, *109*, 393–404.

[12] Maresca, T. J.; Freedman, B. S.; Heald, R. Histone H1 is essential for mitotic chromosome architecture and segregation in Xenopus laevis egg extracts. *J. Cell Biol.* **2005**, *169*, 859–869.

[13] Routh, A.; Sandin, S.; Rhodes, D. Nucleosome repeat length and linker histone stoichiometry determine chromatin fiber structure. *Proc. Natl. Acad. Sci. U.S.A.* **2008**, *105*, 8872–8877.

[14] Hergeth, S. P.; Schneider, R. The H1 linker histones: multifunctional proteins beyond the nucleosomal core particle. *EMBO Rep.* **2015**, *16*, 1439–1453.

[15] Fyodorov, D. V.; Zhou, B. R.; Skoultchi, A. I.; Bai, Y. Emerging roles of linker histones in regulating chromatin structure and function. *Nat. Rev. Mol. Cell Biol.* **2018**, *19*, 192–206.

[16] Fan, Y.; Nikitina, T.; Zhao, J.; Fleury, T. J.; Bhattacharyya, R.; Bouhassira, E. E.; Stein, A.; Woodcock, C. L.; Skoultchi, A. I. Histone H1 depletion in mammals alters global chromatin structure but causes specific changes in gene regulation. *Cell* **2005**, *123*, 1199–1212.

[17] Shen, X.; Gorovsky, M. A. Linker histone H1 regulates specific gene expression but not global transcription in vivo. *Cell* **1996**, *86*, 475–483.

[18] Lu, X.; Wontakal, S. N.; Kavi, H.; Kim, B. J.; Guzzardo, P. M.; Emelyanov, A. V.; Xu, N.; Hannon, G. J.; Zavadil, J.; Fyodorov, D. V. et al. Drosophila H1 regulates the genetic activity of heterochromatin by recruitment of Su(var)3-9. *Science* **2013**, *340*, 78–81.

[19] Lee, H.; Habas, R.; Abate-Shen, C. MSX1 cooperates with histone H1b for inhibition of transcription and myogenesis. *Science* **2004**, *304*, 1675–1678.

[20] Zhang, Y.; Khan, D.; Delling, J.; Tobiasch, E. Mechanisms underlying the osteo- and adipodifferentiation of human mesenchymal stem cells. *ScientificWorldJournal* **2012**, *2012*, 793823.

[21] Christophorou, M. A.; Castelo-Branco, G.; Halley-Stott, R. P.; Oliveira, C. S.; Loos, R.; Radzisheuskaya, A.; Mowen, K. A.; Bertone, P.; Silva, J. C.; Zernicka-Goetz, M. et al. Citrullination regulates pluripotency and histone H1 binding to chromatin. *Nature* **2014**, *507*, 104–108.

[22] Thorslund, T.; Ripplinger, A.; Hoffmann, S.; Wild, T.; Uckelmann, M.; Villumsen, B.; Narita, T.; Sixma, T. K.; Choudhary, C.; Bekker-Jensen, S. et al. Histone H1 couples initiation and amplification of ubiquitin signalling after DNA damage. *Nature* **2015**, *527*, 389–393.

[23] Konishi, A.; Shimizu, S.; Hirota, J.; Takao, T.; Fan, Y.; Matsuoka, Y.; Zhang, L.; Yoneda, Y.; Fujii, Y.; Skoultchi, A. I. et al. Involvement of histone H1.2 in apoptosis induced by DNA double-strand breaks. *Cell* **2003**, *114*, 673–688.

[24] Lever, M. A.; Th'ng, J. P.; Sun, X.; Hendzel, M. J. Rapid exchange of histone H1.1 on chromatin in living human cells. *Nature* **2000**, *408*, 873–876.

[25] Misteli, T.; Gunjan, A.; Hock, R.; Bustin, M.; Brown, D. T. Dynamic binding of histone H1 to chromatin in living cells. *Nature* **2000**, *408*, 877–881.

[26] Catez, F.; Ueda, T.; Bustin, M. Determinants of histone H1 mobility and chromatin binding in living cells. *Nat. Struct. Mol. Biol.* **2006**, *13*, 305–310.

[27] Thoma, F.; Koller, T.; Klug, A. Involvement of histone H1 in the organization of the nucleosome and of the salt-dependent superstructures of chromatin. *J. Cell Biol.* **1979**, *83*, 403–427.

[28] Shimamura, A.; Sapp, M.; Rodriguez-Campos, A.; Worcel, A. Histone H1 represses transcription from minichromosomes assembled in vitro. *Mol. Cell. Biol.* **1989**, *9*, 5573–5584.

[29] Laybourn, P. J.; Kadonaga, J. T. Role of nucleosomal cores and histone H1 in regulation of transcription by RNA polymerase II. *Science* **1991**, *254*, 238–245.

[30] O'Neill, T. E.; Meersseman, G.; Pennings, S.; Bradbury, E. M. Deposition of histone H1 onto reconstituted nucleosome arrays inhibits both initiation and elongation of transcripts by T7 RNA polymerase. *Nucleic Acids Res.* **1995**, *23*, 1075–1082.

[31] Mishra, L. N.; Hayes, J. J. A nucleosome-free region locally abrogates histone H1-dependent restriction of linker DNA accessibility in chromatin. *J. Biol. Chem.* **2018**, *293*, 19191–19200.

[32] McGhee, J. D.; Felsenfeld, G. Nucleosome structure. *Annu. Rev. Biochem.* **1980**, *49*, 1115–1156.

[33] Zhou, B. R.; Jiang, J.; Feng, H.; Ghirlando, R.; Xiao, T. S.; Bai, Y. Structural Mechanisms of Nucleosome Recognition by Linker Histones. *Mol. Cell* **2015**, *59*, 628–638.

[34] Bednar, J.; Garcia-Saez, I.; Boopathi, R.; Cutter, A. R.; Papai, G.; Reymer, A.; Syed, S. H.; Lone, I. N.; Tonchev, O.; Crucifix, C. et al. Structure and Dynamics of a 197 bp Nucleosome in Complex with Linker Histone H1. *Mol. Cell* **2017**, *66*, 384–397.

[35] Syed, S. H.; Goutte-Gattat, D.; Becker, N.; Meyer, S.; Shukla, M. S.; Hayes, J. J.; Everaers, R.; Angelov, D.; Bednar, J.; Dimitrov, S. Single-base resolution mapping of H1-nucleosome interactions and 3D organization of the nucleosome. *Proc. Natl. Acad. Sci. U.S.A.* **2010**, *107*, 9620–9625.

[36] Zhou, B. R.; Feng, H.; Ghirlando, R.; Li, S.; Schwieters, C. D.; Bai, Y. A Small Number of Residues Can Determine if Linker Histones Are Bound On or Off Dyad in the Chromatosome. *J. Mol. Biol.* **2016**, *428*, 3948–3959.

[37] Song, F.; Chen, P.; Sun, D.; Wang, M.; Dong, L.; Liang, D.; Xu, R. M.; Zhu, P.; Li, G. Cryo-EM study of the chromatin fiber reveals a double helix twisted by tetranucleosomal units. *Science* **2014**, *344*, 376–380.

[38] Zhou, B. R.; Feng, H.; Kato, H.; Dai, L.; Yang, Y.; Zhou, Y.; Bai, Y. Structural insights into the histone H1-nucleosome complex. *Proc. Natl. Acad. Sci. U.S.A.* **2013**, *110*, 19390–19395.

[39] Stehr, R.; Kepper, N.; Rippe, K.; Wedemann, G. The effect of internucleosomal interaction on folding of the chromatin fiber. *Biophys. J.* **2008**, *95*, 3677–3691.

[40] Kepper, N.; Foethke, D.; Stehr, R.; Wedemann, G.; Rippe, K. Nucleosome geometry and internucleosomal interactions control the chromatin fiber conformation. *Biophys. J.* **2008**, *95*, 3692–3705.

[41] Perišić, O.; Portillo-Ledesma, S.; Schlick, T. Sensitive effect of linker histone binding mode and subtype on chromatin condensation. *Nucleic Acids Res.* **2019**,

[42] Zhou, B. R.; Jiang, J.; Ghirlando, R.; Norouzi, D.; Sathish Yadav, K. N.; Feng, H.; Wang, R.; Zhang, P.; Zhurkin, V.; Bai, Y. Revisit of Reconstituted 30-nm Nucleosome Arrays Reveals an Ensemble of Dynamic Structures. *J. Mol. Biol.* **2018**, *430*, 3093–3110.

[43] Ozturk, M. A.; Cojocaru, V.; Wade, R. C. Toward an Ensemble View of Chromatosome Structure: A Paradigm Shift from One to Many. *Structure* **2018**, *26*, 1050–1057.

[44] Bascom, G. D.; Schlick, T. Chromatin Fiber Folding Directed by Cooperative Histone Tail Acetylation and Linker Histone Binding. *Biophys. J.* **2018**, *114*, 2376–2385.

[45] Luque, A.; Ozer, G.; Schlick, T. Correlation among DNA Linker Length, Linker Histone Concentration, and Histone Tails in Chromatin. *Biophys. J.* **2016**, *110*, 2309–2319.

[46] Nizovtseva, E. V.; Clauvelin, N.; Todolli, S.; Polikanov, Y. S.; Kulaeva, O. I.; Wengrzynek, S.; Olson, W. K.; Studitsky, V. M. Nucleosome-free DNA regions differentially affect distant communication in chromatin. *Nucleic Acids Res.* **2017**, *45*, 3059–3067.

[47] Öztürk, M. A.; Pachov, G. V.; Wade, R. C.; Cojocaru, V. Conformational selection and dynamic adaptation upon linker histone binding to the nucleosome. *Nucleic Acids Res.* **2016**, *44*, 6599–6613.

[48] Ozturk, M. A.; Cojocaru, V.; Wade, R. C. Dependence of Chromatosome Structure on Linker Histone Sequence and Posttranslational Modification. *Biophys. J.* **2018**, *114*, 2363–2375.

[49] Ramakrishnan, V.; Finch, J. T.; Graziano, V.; Lee, P. L.; Sweet, R. M. Crystal structure of globular domain of histone H5 and its implications for nucleosome binding. *Nature* **1993**, *362*, 219–223.

[50] Pachov, G. V.; Gabdoulline, R. R.; Wade, R. C. On the structure and dynamics of the complex of the nucleosome and the linker histone. *Nucleic Acids Res.* **2011**, *39*, 5255–5263.

[51] Brown, D. T.; Izard, T.; Misteli, T. Mapping the interaction surface of linker histone H1(0) with the nucleosome of native chromatin in vivo. *Nat. Struct. Mol. Biol.* **2006**, *13*, 250–255.

[52] Bharath, M. M.; Chandra, N. R.; Rao, M. R. Molecular modeling of the chromatosome particle. *Nucleic Acids Res.* **2003**, *31*, 4264–4274.

[53] Zhou, Y. B.; Gerchman, S. E.; Ramakrishnan, V.; Travers, A.; Muyldermans, S. Position and orientation of the globular domain of linker histone H5 on the nucleosome. *Nature* **1998**, *395*, 402–405.

[54] George, E. M.; Izard, T.; Anderson, S. D.; Brown, D. T. Nucleosome interaction surface of linker histone H1c is distinct from that of H1(0). *J. Biol. Chem.* **2010**, *285*, 20891–20896.

[55] Davey, C. A.; Sargent, D. F.; Luger, K.; Maeder, A. W.; Richmond, T. J. Solvent mediated interactions in the structure of the nucleosome core particle at 1.9 a resolution. *J. Mol. Biol.* **2002**, *319*, 1097–1113.

[56] Dorigo, B.; Schalch, T.; Kulangara, A.; Duda, S.; Schroeder, R. R.; Richmond, T. J. Nucleosome arrays reveal the two-start organization of the chromatin fiber. *Science* **2004**, *306*, 1571–1573.

[57] Thastrom, A.; Bingham, L. M.; Widom, J. Nucleosomal locations of dominant DNA sequence motifs for histone-DNA interactions and nucleosome positioning. *J. Mol. Biol.* **2004**, *338*, 695–709.

[58] Sali, A.; Blundell, T. L. Comparative protein modelling by satisfaction of spatial restraints. *J. Mol. Biol.* **1993**, *234*, 779–815.

[59] Pettersen, E. F.; Goddard, T. D.; Huang, C. C.; Couch, G. S.; Greenblatt, D. M.; Meng, E. C.; Ferrin, T. E. UCSF Chimera–a visualization system for exploratory research and analysis. *J Comput Chem* **2004**, *25*, 1605–1612.

[60] Wriggers, W. Conventions and workflows for using Situs. *Acta Crystallogr. D Biol. Crystallogr.* **2012**, *68*, 344–351.

[61] Wriggers, W.; Milligan, R. A.; McCammon, J. A. Situs: A package for docking crystal structures into low-resolution maps from electron microscopy. *J. Struct. Biol.* **1999**, *125*, 185–195.

[62] Lopez-Blanco, J. R.; Garzon, J. I.; Chacon, P. iMod: multipurpose normal mode analysis in internal coordinates. *Bioinformatics* **2011**, *27*, 2843–2850.

[63] Case, D. A.; Betz, R. M.; Cerutti, D. S.; Cheatham, T. E.; Darden, T. A.; Duke, R. E.; Giese, T. J.; Gohlke, H.; Goetz, A. W.; Homeyer, N. et al. *AMBER 2016*; University of California, San Francisco, 2016.

[64] Jorgensen, W. L.; Chandrasekhar, J.; Madura, J. D.; Impey, R. W.; Klein, M. L. Comparison of simple potential functions for simulating liquid water. *J Chem Phys* **1983**, *79*, 926–935.

[65] Mahoney, M. W.; Jorgensen, W. L. A five-site model for liquid water and the reproduction of the density anomaly by rigid, nonpolarizable potential functions. *J Chem Phys* **1983**, *112*, 8910–8922.

[66] Maier, J. A.; Martinez, C.; Kasavajhala, K.; Wickstrom, L.; Hauser, K. E.; Simmerling, C. ff14SB: Improving the Accuracy of Protein Side Chain and Backbone Parameters from ff99SB. *J Chem Theory Comput* **2015**, *11*, 3696–3713.

[67] Ivani, I.; Dans, P. D.; Noy, A.; Perez, A.; Faustino, I.; Hospital, A.; Walther, J.; Andrio, P.; Goni, R.; Balaceanu, A. et al. Parmbsc1: a refined force field for DNA simulations. *Nat. Methods* **2016**, *13*, 55–58.

[68] Phillips, J. C.; Braun, R.; Wang, W.; Gumbart, J.; Tajkhorshid, E.; Villa, E.; Chipot, C.; Skeel, R. D.; Kale, L.; Schulten, K. Scalable molecular dynamics with NAMD. *J Comput Chem* **2005**, *26*, 1781–1802.

[69] Darden, T.; York, D.; Pedersen, L. Particle mesh Ewald: An Nlog(N) method for Ewald sums in large systems. *J. Chem. Phys.* **1993**, *98*, 10089–10092.

[70] Hoover, W. G. Canonical dynamics: Equilibrium phase-space distributions. *Phys Rev A Gen Phys* **1985**, *31*, 1695–1697.

[71] Towns, J.; Cockerill, T.; Dahan, M.; Foster, I.; Gaither, K.; Grimshaw, A.; Hazlewood, V.; Lathrop, S.; Lifka, D.; Peterson, G. et al. XSEDE: accelerating scientific discovery. *Computing in Science & Engineering* **2014**, *16*, 62–74.

[72] Darve, E.; Rodriguez-Gomez, D.; Pohorille, A. Adaptive biasing force method for scalar and vector free energy calculations. *J Chem Phys* **2008**, *128*, 144120.

[73] Henin, J.; Fiorin, G.; Chipot, C.; Klein, M. L. Exploring Multidimensional Free Energy Landscapes Using Time-Dependent Biases on Collective Variables. *J Chem Theory Comput* **2010**, *6*, 35–47.

[74] Fu, H.; Shao, X.; Chipot, C.; Cai, W. Extended Adaptive Biasing Force Algorithm. An On-the-Fly Implementation for Accurate Free-Energy Calculations. *J Chem Theory Comput* **2016**, *12*, 3506–3513.

[75] Humphrey, W.; Dalke, A.; Schulten, K. VMD: visual molecular dynamics. *J Mol Graph* **1996**, *14*, 33–38.

[76] Miller, B. R.; McGee, T. D.; Swails, J. M.; Homeyer, N.; Gohlke, H.; Roitberg, A. E. MMPBSA.py: An Efficient Program for End-State Free Energy Calculations. *J Chem Theory Comput* **2012**, *8*, 3314–3321.

[77] Nguyen, H.; Perez, A.; Bermeo, S.; Simmerling, C. Refinement of Generalized Born Implicit Solvation Parameters for Nucleic Acids and Their Complexes with Proteins. *J Chem Theory Comput* **2015**, *11*, 3714–3728.

[78] Johnson, S. C. Hierarchical clustering schemes. *Psychometrika* **1967**, *32*, 241–254.

[79] Kvålseth, T. O. On Normalized Mutual Information: Measure Derivations and Properties. *Entropy* **2017**, *631*, 1–14.

[80] McClendon, C. L.; Hua, L.; Barreiro, A.; Jacobson, M. P. Comparing Conformational Ensembles Using the Kullback-Leibler Divergence Expansion. *J Chem Theory Comput* **2012**, *8*, 2115–2126.

[81] Piana, S.; Donchev, A. G.; Robustelli, P.; Shaw, D. E. Water dispersion interactions strongly influence simulated structural properties of disordered protein states. *J Phys Chem B* **2015**, *119*, 5113–5123.

[82] Battiste, J. L.; Wagner, G. Utilization of site-directed spin labeling and high-resolution heteronuclear nuclear magnetic resonance for global fold determination of large proteins with limited nuclear overhauser effect data. *Biochemistry* **2000**, *39*, 5355–5365.

[83] Clore, G. M. Practical Aspects of Paramagnetic Relaxation Enhancement in Biological Macromolecules. *Meth. Enzymol.* **2015**, *564*, 485–497.

[84] Miller, B. R.; McGee, T. D.; Swails, J. M.; Homeyer, N.; Gohlke, H.; Roitberg, A. E. MMPBSA.py: An Efficient Program for End-State Free Energy Calculations. *J Chem Theory Comput* **2012**, *8*, 3314–3321.

[85] Hou, T.; Wang, J.; Li, Y.; Wang, W. Assessing the performance of the MM/PBSA and MM/GBSA methods. 1. The accuracy of binding free energy calculations based on molecular dynamics simulations. *J Chem Inf Model* **2011**, *51*, 69–82.

[86] Genheden, S.; Ryde, U. The MM/PBSA and MM/GBSA methods to estimate ligand-binding affinities. *Expert Opin Drug Discov* **2015**, *10*, 449–461.